

Re-arrangements of 4-[(4H-1,2,4-triazol-4-ylimino)methyl]phenol with different inorganic anions: Crystal structure and fluorescence properties



Ya-Wen Zhang, Jing-Wen Wang, Hong-Shuai Wu, Ming-Xin Wang, Yang-Hui Luo*, Bai-Wang Sun*

School of Chemistry and Chemical Engineering, Southeast University, Nanjing 211189, PR China

ARTICLE INFO

Article history:

Received 13 April 2017

Accepted 18 May 2017

Available online 30 May 2017

Keywords:

Re-arrangements
Inorganic-anions
Organic salts
Optical-properties
Schiff base

ABSTRACT

Fluorescent materials have many interesting applications, but it remains difficult to control the luminescence of organic materials and in particular to retain the same luminescence in solution and in the solid state, a property of interest for various imaging applications. In this work, the influence of inorganic-anions on the crystal structure and physical-chemical properties of a series organic salts L^+Cl^- (**1**), $L^+ClO_4^-$ (**2**), $L^+NO_3^- \cdot H_2O$ (**3**), $2L^+SO_4^{2-} \cdot 2H_2O$ (**4**) ($L = 4-[(4H-1,2,4-triazol-4-ylimino)methyl]phenol$) has been investigated. Single crystal X-ray analyzes revealed that salt **1** formed a linear structure connected by $H \cdots O$ interactions, while salts **2–4** all formed 2D network structures through $O \cdots O$ interactions. The protonated L^+ s adopt face-to-face slipped π -stacked arrangement in salts **1** and **3**, while display monomer arrangements in **2** and **4**, the latter can be attribute to the entrapment of heavy anions in the crystal lattices. Optical-properties measurements of these four salts have shown L^+ arrangements dependent on solid-state properties: salt **1** and **3** show broad emission bands ($\lambda_1 = 478$ nm, $\lambda_2 = 487$ nm) with a red shift of about 60 nm relative to its fluorescence in solvents, while **2** and **4** are similar to each other, exhibiting sharp bands ($\lambda_3 = 453$ nm, $\lambda_2 = 433$ nm) with the higher ϕ_{PL} values ($\phi_{PL1} = 0.08$, $\phi_{PL1} = 0.15$, $\phi_{PL1} = 0.06$, $\phi_{PL1} = 0.14$). These results demonstrated the significant influence of inorganic-anions on the organic salts and the optical properties of organic materials could be modulated by entrapping different anions in lattice.

© 2017 Elsevier Ltd. All rights reserved.

1. Introduction

Systematic structural variation of fluorescent organic molecules plays a vital role in solid for the enhancement of emission properties. In recent years, the design and synthesis of organic solid-state fluorescence materials as well as promising optoelectronic applications in lasers [1], sensors [2], organic light-emitting diodes [3] and two-photon fluorescent materials [4] have attracted great attention. From the previous study, many organic fluorophores have strong fluorescence in solution while losing this property in the solid state [5,6].

Co-crystals deal with the design, synthesis, and evaluation of solid-state supramolecular structures with tailored form and function [7], that is, from the designed chemistry of intermolecular forces to materials with, hopefully, desired fine-tuning properties by modulating the π -conjugated molecule structure [8,9]. Co-crystals remain neutral while crystallizing together, whereas an organic salt is usually formed due to a proton exchange within

the complex between an acid and a base [10–12]. The advantage of an organic salt over neutral molecules in a co-crystal is the strong hydrogen bonding, which controls the molecular assembly tailoring the properties of solid-state materials. Consequently, the molecular tailorability of promising molecules exhibiting fluorescence has attracted considerable attention [13].

Triazole class is a rich N-containing heterocycle comprising of three nitrogen and two carbon atoms [14], which has received attention as a novel non-toxic chemical compound [15]. Heterocyclic compounds especially 4-Amino-1,2,4-triazoles and their condensed derivatives [16] have been used as excellent candidates for the construction of medicine and pesticide intermediates [17]. The fluorescence properties of 4-Amino-1,2,4-triazoles is very weak, however, after introducing aromatic aldehyde, the fluorescence efficiency increases due to the higher conjugate degree and the presence of hydroxyl having a good coordination ability. The photometric, electrochemical and thermochromic properties [18] of triazol containing Schiff base and phenol moieties allow their applications in potentiometric sensors [19], molecular electronic devices [20], optical computers [21], imaging systems [22], molecular memory storage devices [23] and as photodetectors in biological systems [24].

* Corresponding authors. Fax: +86 25 52090614.

E-mail addresses: peluoyh@sina.com (Y.-H. Luo), chmsunbw@seu.edu.cn (B.-W. Sun).

Because of their interesting architectures and applications in diverse areas, 4-[(4H-1,2,4-triazol-4-ylimino)methyl]phenol (**L**, Scheme 1) was used as organic ligand in our efforts. **L** can be coordinated to metal ions in different modes, bidentate bridging or monodentate, depending on the nature of the substituent group at the triazole ring [25]. Besides, the complexes with different nuclearity have been obtained depending on variables such as the co-ligand, anion and the metal–ligand ratio [26]. The salt formation of **L** with inorganic anions has not been investigated yet. Hence, this paper discusses the arrangements of **L** molecules by formation of its different salts and the influence of inorganic anions in crystal structures and physical properties. Four acids, Hydrobromic acid (HCl), perchloric acid (HClO₄), nitric acid (HNO₃) and sulfuric acid (H₂SO₄) were used as hydrogen bond donors, and O–H···O hydrogen bonds would be expected to be formed with the hydroxyl group as hydrogen bond acceptors. In this work, we obtained four organic salts: L⁺Cl[−] (**1**), L⁺ClO₄[−] (**2**), L⁺NO₃[−]·H₂O (**3**), 2L⁺SO₄^{2−}·2H₂O (**4**). By entrapment of different anions in the lattice, the stacking modes changed greatly, which afforded the different properties in solid state. These salts were characterized by single-crystal X-ray diffraction, molecular Hirshfeld surfaces and physical measurements (differential scanning calorimetry (DSC), thermogravimetric analyzes (TGA), infrared absorption spectroscopy (IR)). We further analyzed absorption spectra (UV–Vis, diffuse reflectance spectra) and fluorescence of the four salts.

2. Results and discussion

2.1. Crystal structures

The crystal structures of **1–4** were elucidated by single crystal X-ray diffraction and the crystallographic data are presented in Table 1

2.1.1. L⁺Cl[−] (**1**)

Organic salt **1** crystallizes as brown cuboid-shaped crystals. The structural determination shows **1** forms a 1:1 (L⁺: Cl[−]) salt in the Triclinic *P* $\bar{1}$ space group with *Z* = 2. Fig. 1a shows the asymmetric unit (ASU) of **1** consists of an entire molecule of L⁺ cation and one Cl[−] anion, and selected bond distances and angles are tabulated in Table 2. In the structure, the L⁺ and Cl[−] associate through the O–H···Cl (distance of 3.125 Å) and N–H···Cl (distance of 3.024 Å) hydrogen bonds to form the infinite 1D chains (Fig. 1b). As shown in Fig. 1c, the two neighboring chains are linked by π – π interactions between the rings, and the plane separation of the double-decker is 3.563 Å.

2.1.2. L⁺ClO₄[−] (**2**)

Organic salt **2** crystallizes as brown needlelike crystals. And it forms in the monoclinic *P*2₁/*c* space group with *Z* = 4. The structural determination shows that **2** forms a 1:1 (L⁺: ClO₄[−]) salt and has an entire molecule of L⁺ ClO₄[−] in the ASU (Fig. 2a). L⁺ cation and ClO₄[−] anion are connected through N–H···O (distance of 2.672 Å) and O–H···O (distance of 2.568 Å) hydrogen bonds (Fig. 2b). As illustrated in Fig. 2c, L⁺ and ClO₄[−] associate alternately through O···O interactions (distance of 2.897 Å) to construct R₂²(6) pramolecular synthons. Despite the abundance of aromatic rings in the crystal structure, no significant intermolecular π ··· π or

C–H··· π interactions have been detected, due to the separating action of the perchlorate ions (Fig. 2d).

2.1.3. L⁺NO₃[−]·H₂O (**3**)

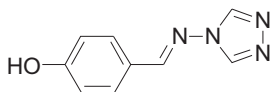
Organic salt **3** crystallizes as a brown needlelike crystal and has a monoclinic system and space group *P*2₁/*c* with *Z* = 4. In particular, the asymmetric unit of **3** consists of one protonated L⁺, one NO₃[−] anion and a solvent site H₂O, which is different from **1** and **2** (Fig. 3a). L⁺ and NO₃[−] are connected by O–H···O (distance of 2.719 Å for the hydroxyl group) hydrogen bonding interactions. In addition, water molecules play the major role in the supramolecular 3D organization of the structure. Through their oxygen atoms acting as multihydrogen-bonded acceptors, the water molecules link neighboring L⁺ and NO₃[−] units of the structure by means of N–H···O and O–H···O hydrogen bonds. The adjacent 1D chains in one plane are connected with each other by R₂⁴(12) pramolecular synthons through π – π (distance of 2.812 and 2.891 Å) intermolecular interactions between oxygen atoms of NO₃[−] and H₂O molecules into 2D structure (Fig. 3b). The packing of **3** are stacked in a parallel fashion, in which the rings adopt a face-to-face slipped π -stacked arrangement. The closest plane separation between the neighboring moieties is 3.398 Å, which is shorter than **2** could due to the addition of water molecules (Fig. 3c).

2.1.4. 2L⁺SO₄^{2−}·2H₂O (**4**)

Organic salt **4**, brown needlelike crystals, crystallizes in monoclinic *C**c* space group with *Z* = 4. The ASU consists of an entire molecule of two L⁺ cations, one SO₄^{2−} anion and two H₂O molecules (Fig. 4a), which is similar to **3**. The hydrogen bonds linked to the cation, which have N1 and N5 as the donors, are attached to one sulfate anions and have length of 2.630 Å. The other hydrogen bond of a dimer unit has a donor–acceptor distance of 2.635 Å (Fig. 4b). Each of the dimeric units is stacked through the O···O interactions, in which **L** molecules are widely separated and no π – π interaction between the two ring fluorophores (the closest distance between two parallel rings is 5.392 Å), which is different from crystal **3** may due to the heavy atoms of SO₄^{2−} (Fig. 4c).

2.2. Hirshfeld surface calculation

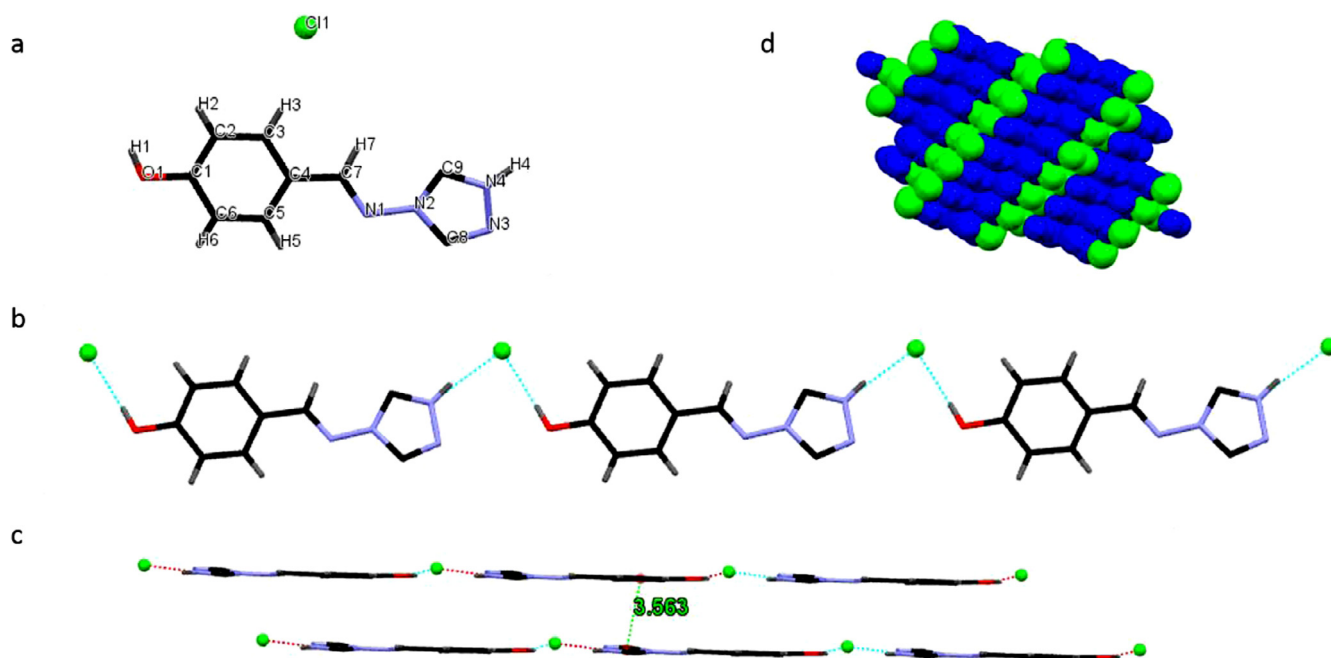
Molecular Hirshfeld surface is a powerful tool for gaining additional insight into crystal structure and polymorph comparison by color-coding short or long contacts. 3D color-coding scheme can give intermolecular interactions, and it can be resolved into 2D fingerprint plots, which give a quantitatively summary of the nature and type of intermolecular contacts experienced by the molecules in the crystal [27]. The 3D Hirshfeld surfaces and 2D fingerprint plots of four organic salts are shown in Fig. 5, which clearly show the similarities and differences of the influences of different anions on the intermolecular interactions of the **L** molecule. For salt **1**, the large red region in the middle of the dnorm surface corresponding to both donor and acceptor of the O–H···Cl hydrogen bond, represents the ligand molecule connecting with Cl into the linear structure. For **2–4**, the closest intermolecular interactions are all found to be O–H···O and N–H···O interactions and have a most significant contribution to the total Hirshfeld surfaces, indicating the formation of hydrogen bonds. The hotspots on the 2D fingerprint plots are represent the close intermolecular interactions. The differences in the 3D dnorm and 2D fingerprint plots of salts **1–4** indicate visually that the introduction of anions exerts a significant influence on the types and numbers of intermolecular interactions. Then, the problem arises how intermolecular interactions vary quantitatively. To answer it, relative contributions of different



Scheme 1. Chemical structure of **L**.

Table 1
Crystal data and structure refinement for salts **1–4**.

Salt	1	2	3	4
Formula	C ₉ H ₇ ClN ₄ O	C ₉ H ₉ ClN ₄ O ₅	C ₆ H ₉ N ₂ O ₂	C ₁₈ H ₂₂ N ₈ O ₈ S
Formula weight	222.64	288.65	269.23	510.50
Crystal system	triclinic	monoclinic	monoclinic	monoclinic
Space group	<i>P</i> $\bar{1}$	<i>P</i> 2 ₁ / <i>c</i>	<i>P</i> 2 ₁ / <i>c</i>	<i>C</i> 2
<i>a</i> (Å)	6.4952(13)	7.1870(14)	7.1440(14)	6.7700(14)
<i>b</i> (Å)	7.5138(15)	16.366(3)	18.168(4)	20.084(4)
<i>c</i> (Å)	10.839(2)	10.661(2)	9.3760(19)	16.848(3)
α (°)	97.30(3)	90.00	90.00	90.00
β (°)	93.46(3)	95.43(3)	104.84(3)	101.50(3)
γ (°)	102.79(3)	90.00	90.00	90.00
<i>V</i> (Å ³)	509.54(19)	1248.3(4)	1176.3(4)	2244.9(8)
<i>Z</i>	2	4	4	4
<i>D</i> _{calc} (mg m ⁻³)	1.451	1.536	1.520	1.510
<i>T</i> (K)	293(2)	293(2)	293(2)	293(2)
μ (mm ⁻¹)	0.352	0.329	0.126	0.208
Cryst dimensions	0.2 × 0.25 × 0.32	0.3 × 0.25 × 0.3	0.3 × 0.3 × 0.4	0.3 × 0.2 × 0.25
No. of reflections collected	2263	2298	2108	2266
No. of unique reflections	1942	967	1381	1466
No. of parameters	137	172	172	316
Goodness-of-fit (GOF) on <i>F</i> ²	1.093	0.973	1.004	1.002
<i>R</i> ₁ , <i>wR</i> ₂ (<i>I</i> > 2 σ (<i>I</i>))	0.0533, 0.1610	0.0904, 0.1664	0.0661, 0.1644	0.0548, 0.1059
<i>R</i> ₁ , <i>wR</i> ₂ (all data)	0.0603, 0.1679	0.2150, 0.2116	0.1022, 0.1848	0.1002, 0.1243
CCDC NO.	1524375	1524377	1524379	1524378

**Fig. 1.** (a) Molecular structure of salt **1**, (b) Hydrogen bonds between the L⁺ and Cl⁻ molecules, (c) Double-decker structure of **1**, the plane separation is highlighted, (d) Spacefill model of **1** (L⁺ and Cl⁻ are indicated by blue and green). (Color online.)**Table 2**
Geometrical parameters for the hydrogen bonds in salts.

Salt	D–H (Å)	H...A (Å)	D–A (Å)	\angle D–H...A (°)
1				
O1–H1...Cl1	0.820	2.310	3.125	172.8
N4–H4...Cl1	0.861	2.179	3.024	167.2
2				
O1–H1A...O5	0.851	1.719	2.568	175.2
N2–H2...O4	0.860	1.813	2.672	179.1
3				
O1–H1A...O5	0.820	1.899	2.719	178.3
N1–H1B...OW	0.861	1.814	2.643	161.2
4				
O1–H1A...OW1	0.821	1.822	2.635	170.0
N1–H1B...O4	0.859	1.777	2.630	169.2

intermolecular interactions to the Hirshfeld surface are summarized in Fig. 6.

2.3. Thermal behavior

Thermal studies over the Schiff base ligand and their salts, through the thermogravimetric (TGA-DTG) (Fig. 7) and differential scanning calorimetric (DSC) (Fig. 1S) techniques, were investigated. And the obtained weight loss data of L and four salts are tabulated in Table 3. From the curves, it can be seen that the addition of HCl, HClO₄, HNO₃ and H₂SO₄ can affect the pyrolysis. The data indicate that the ligand and salts **1–4** start decomposition at 272, 233, 235, 240 and 230 °C, respectively. The points of salts **1–4** are lower than L, which may attribute to the hydrogen bonds

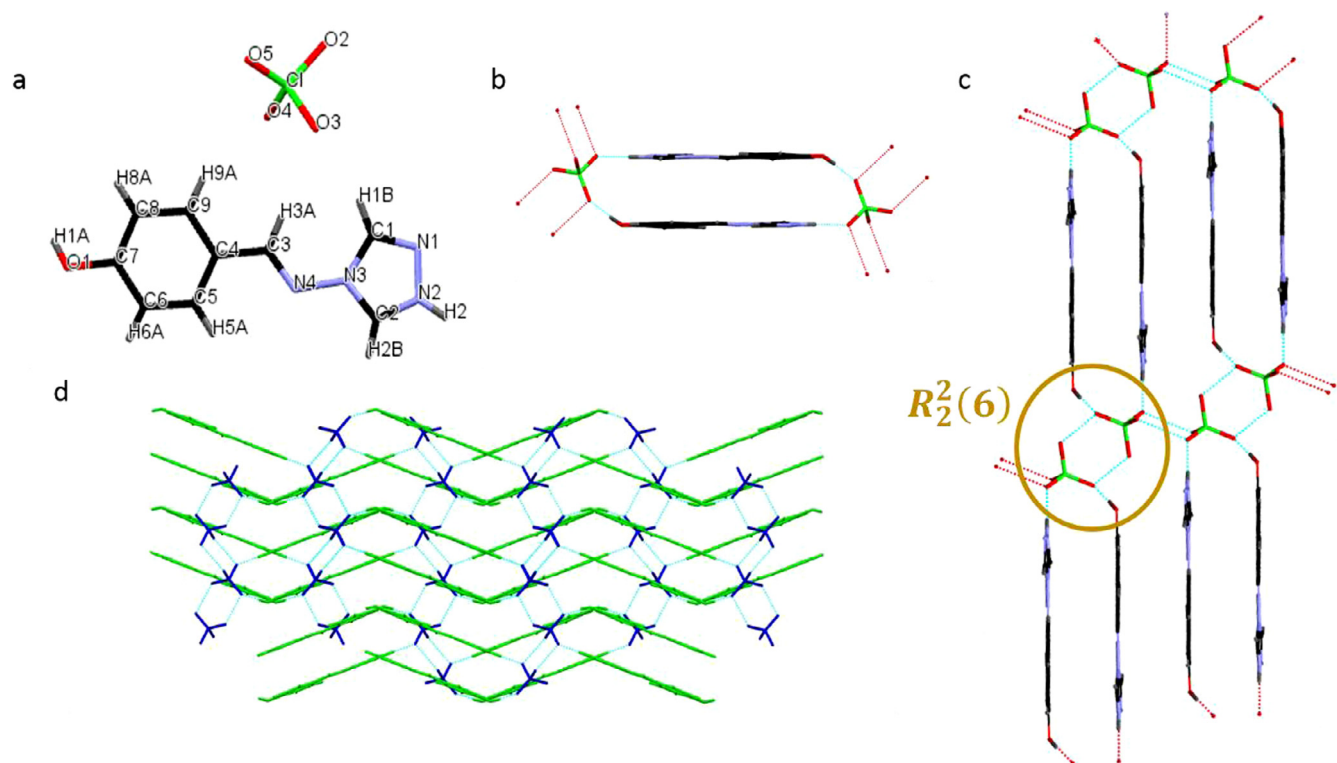


Fig. 2. (a) Molecular structure of salt **2**, (b) Hydrogen bonds between the L^+ and ClO_4^- molecules, (c) Supramolecular synthons around the L^+ unit and the ClO_4^- molecule, (d) Stacking structure of **2** (L^+ and ClO_4^- are indicated by green and blue). (Color online.)

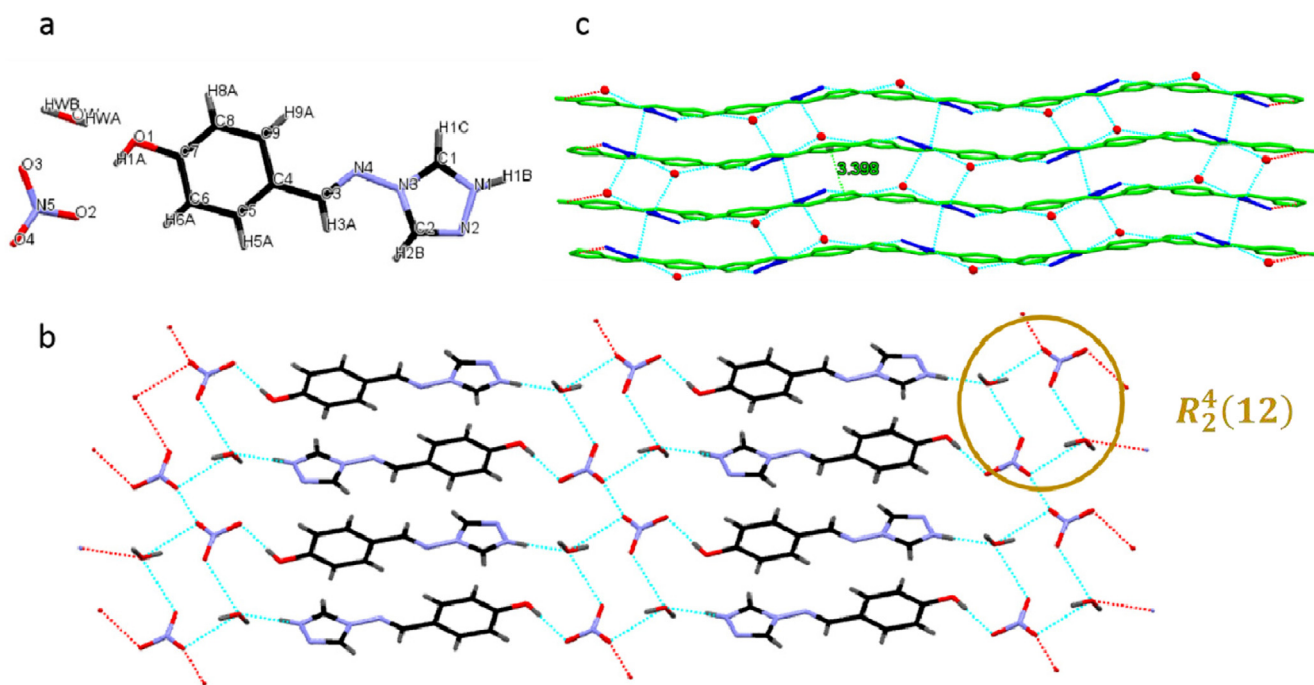


Fig. 3. (a) Molecular structure of salt **3**, (b) Supramolecular synthons around the L^+ , NO_3^- and H_2O , (c) The packing of **3** (L^+ , NO_3^- and H_2O are indicated by green, blue, red). (Color online.)

and weak contacts between the triazole rings in their crystals. For **1** and **2**, the stage occurred from 200 to 400 °C with over 80% mass loss, corresponding to the release of the *p*-Hydroxybenzaldehyde from Schiff base. During this process the C=N of Schiff base may be completely broken. Salts **3** and **4** show two steps of mass loss,

the first pronounced mass loss step is in temperature range of 100–130 °C (the yellow square), which refer to the decomposition of salts and lattice water molecule (mass loss 10%), the second decomposition is in temperature range of 200–400 °C with loss of 40%, indicating the decomposition of **L**, which is the same to **2**,

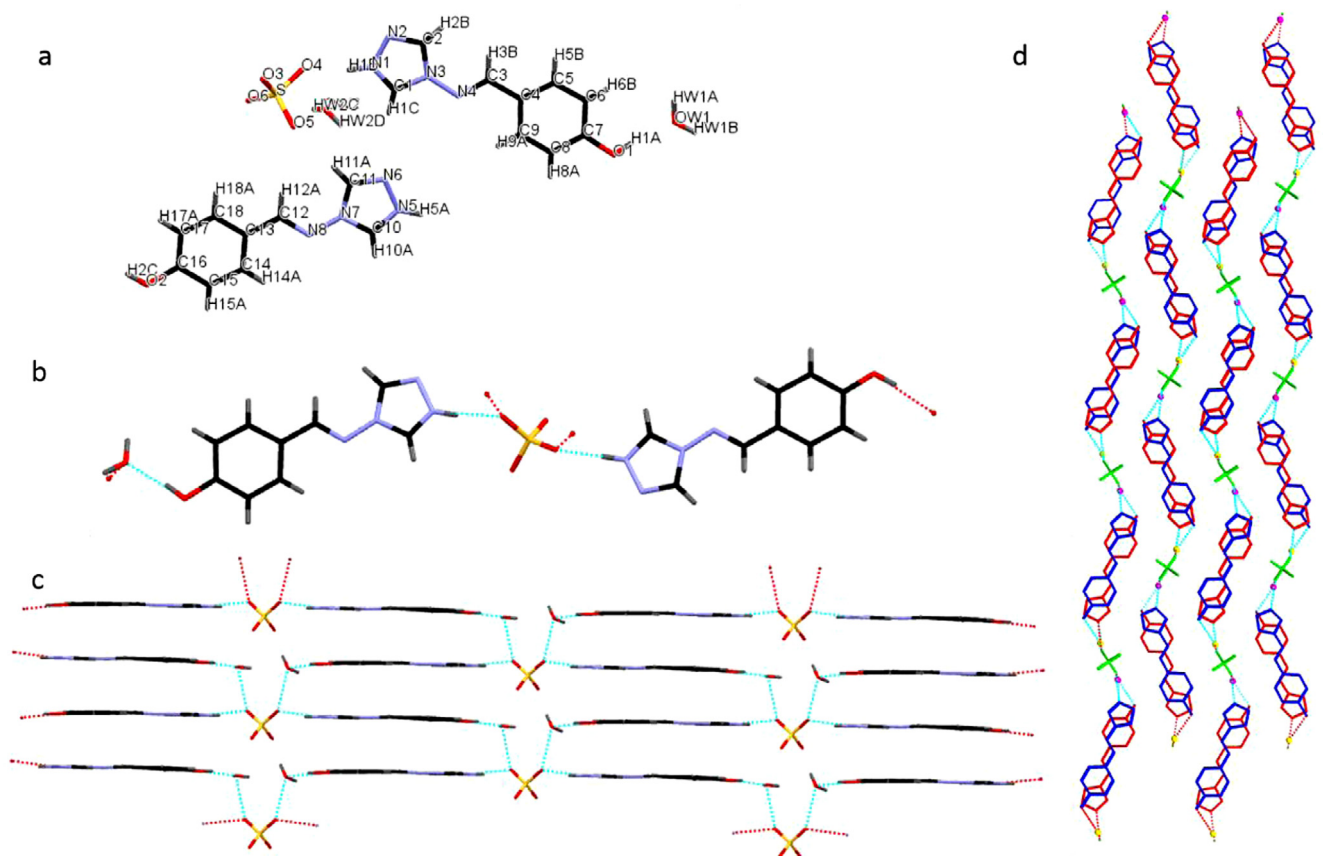


Fig. 4. (a) Molecular structure of salt **4**, (b) Dimeric units of L^+ , NO_3^- and H_2O , (c) 2D chain motif of **4**, (d) The packing motif of **4** (L^+ , SO_4^{2-} and H_2O are indicated by red (blue), green, yellow (purple)). (Color online.)

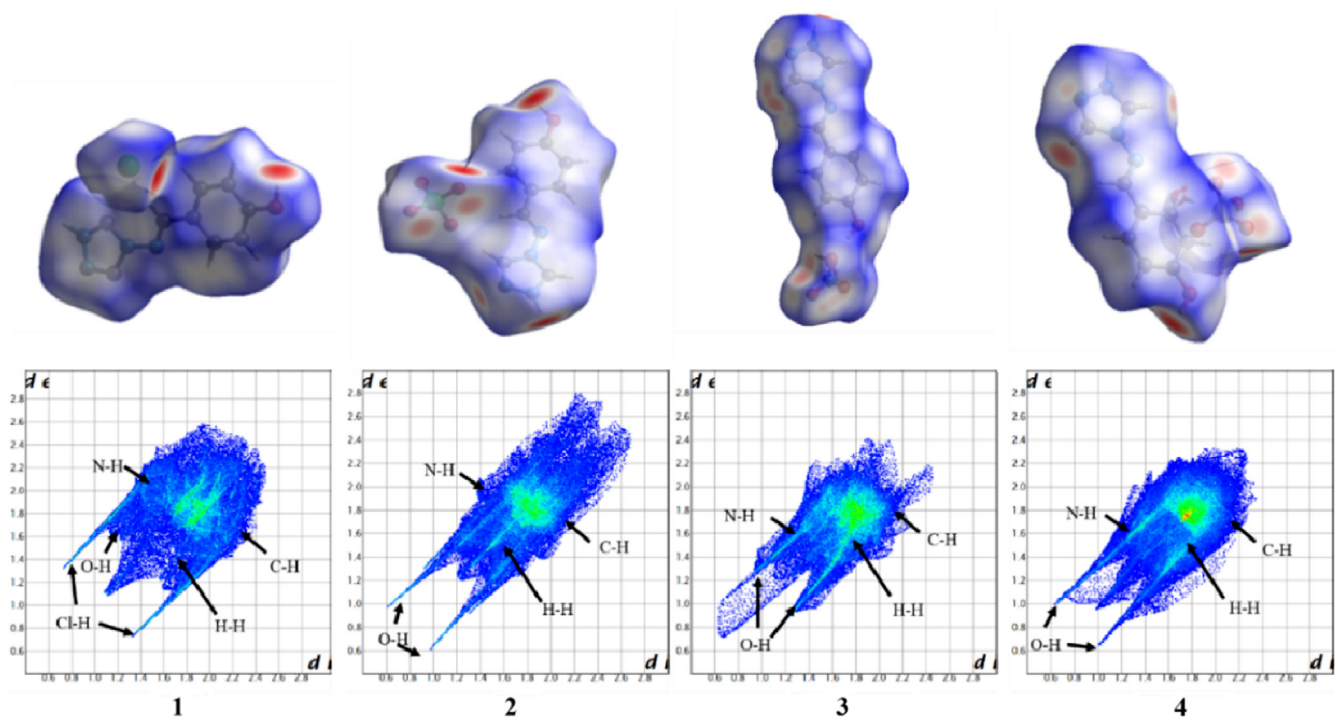


Fig. 5. Hirshfeld surfaces (top) and fingerprint plots (bottom) for salts **1–4**.

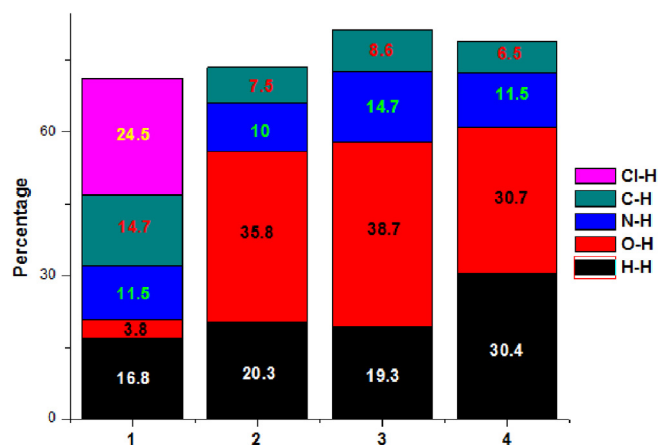


Fig. 6. The percentage contributions from individual intermolecular interactions to the Hirshfeld surfaces of salts 1–4.

3 and **L**. Notably, the DSC curves of **2**, **3** and **4** show obvious peaks at the temperature region from 130 to 150 °C, which may be relative to the melting point of acids. But the curve of **1** at this region is flat, probably due to the linear structure.

2.4. FT-IR spectroscopy

The FT-IR spectrum of **L** and salts **1–4** shows several characteristic stretching vibration modes due to O–H, N–H, CH=N, C–N and N–N bands, as shown in Fig. 8. There are distinct differences in the band characteristics between **L** and four salts. FT-IR spectrum of **L** shows additional bands, ~ 3420 , ~ 1598 , ~ 1505 and ~ 1050 cm^{-1} corresponding to O–H, CH=N, C–N and N–N bonds respectively. Salts **1–4** show boarder absorption peaks around 3400 cm^{-1} attribute to stretching vibration of O–H groups due to stronger hydrogen bond interactions than in **L**. In four salts, the N–H stretching frequency of the salts was used as a probe to identify the proton displacement. The acid–base interaction involving the proton transfer gives rise to a hydrogen bond, and it appears as a broad and medium-strong band at about 3080 cm^{-1} from the Fig. 8. This band is due to the N–H⁺ stretching vibration of the salt, occurring in the 3300 – 2370 cm^{-1} region [28]. In all salts, the imine bands appeared in the region from 1603 to 1620 cm^{-1} [29a] and the triazole (1510 cm^{-1}) C–N stretching bands are shown in ~ 1510 cm^{-1} [29b]. This was evident from a comparison of intensities of the N–N peak (1050 cm^{-1}). A ratio of 0.5 was noticed for four salts, which is result of hydrogen bonds between **L** and anions [29b]. These differences provide a proof of the formation of hydrogen bonds.

2.5. Absorption spectra and fluorescence emission spectra

The UV–Vis spectroscopic measurements were done for exploring the structural differences of four organic salts and their raw material in methanol solution (concentration of 10–4 g/ml) by correlating the absorption spectra recorded (Fig. 9a). The four salts are all shown maximum absorption around 310 nm and other absorption peaks around 203 nm and 230 nm, which are almost identical with ligand except the increase of intensity. Previous studies revealed that triazolic chromophore absorbs around 205 nm [30]. Hence, the absorption peaks of all our selected crystals (227 nm) are attributable to π – π^* transition of triazolic moiety. The corresponding redshift observed in the spectra of all these compounds in comparison to triazole might be due to the attached aromatic system. The intense absorption band appearing around 308 nm in the spectra can be attributed to the π – π^* transitions of the

phenolic ring and associated conjugated segment up to azomethine group of these compounds.

As typical π -conjugated molecules, **L** and salts have displayed a potential value in the field of optics. Therefore, the photophysical properties of the four salts have been further investigated and compared to disclose the influence of different anions on the optical properties of **L**, which would be beneficial for exploring new materials. In order to better understand the influence of intermolecular interactions and stacking models on the photophysical properties of crystals, fluorescence emission spectra were exploited to investigate the optical-properties of the crystals.

The diffuse reflectance spectra (DRS) as pure solid powders to avoid matrix and environment effects [31], each exhibit bands exclusively in the UV region (Fig. 9b), which is typical of the enol form. Similarly, the solids (four salts and **L**) show broad bands with fine peaks (225 nm, 300 nm, 363 nm) arising from triazole and phenolic ring, corresponding to the spectra of compounds in the solvents. However, for the four salts, the main absorption peaks red shift compared with the **L** due to intermolecular hydrogen bond interactions. Thus we may conclude that the formation of hydrogen bond interactions lead to red shift.

The fluorescence emission spectra of the five compounds in methanol are shown in Fig. 10a. All the compounds exhibited emissions with maximum peaks (λ_{max}) at around 420 nm in solution.

By comparing the absorption spectra and fluorescence emission spectra of the five compounds in solution, it can be seen that the absorption and fluorescent emissions of the four salts are probably assigned to the intraligand fluorescent emission because similar behaviors are also observed for the free ligand in methanol solution. In present study, metal–ligand complexes have been synthesized and characterized. The conclusion showed that the fluorescence peak of these complexes were same as **L** and the red-shift is based on metal-to-ligand charge transfer [26]. However, the emissions of **1–4** in solution are slightly blue-shifted, which are attributed to intermolecular hydrogen bond interactions of **L** and anions. The blue shift of photoluminescence suggests that ligand in salts are in higher conjugated level, which increases with the enhancement of conjugated structures [32].

Compared with the similar photophysical properties with maximum fluorescence peaks (λ_{max}) around 420 nm in methanol solution, the fluorescence spectra of all the salts **1–4** in the solid state display strong and red-shifted emissions (Fig. 10b). The emissions in solution should be related to the conjugated configuration and the corresponding intramolecular rotational motions around the double bonds beside the conjugate moieties. These intramolecular motions can lead to fast non-radiative relaxation in solution [33]. In addition, in the crystalline state, intramolecular vibrational relaxation is effectively inhibited, leading to the closure of the non-radiative decay channel, which would cause the strong shifted emissions in the crystalline state compared with those in solution [34].

Organic salts **1** and **3** exhibit a broader emission band located at 470–450 nm, which are ascribed to phenolic ring and triazole fluorophores. The strongest peaks of **2** and **4** are blue-shifted to 455 and 435 nm, which indicates that different types of electronically excited states exist for these salts [35]. It also implies different anions have different influence on the fluorescence properties of **L** in crystalline. The vibrational fine structures appear in the fluorescence spectrum of **2** and **4**, which is the similar image of the absorption spectrum of **2** and **4** in the range from 380 to 600 nm and can be ascribed to the transitions from the lowest vibrational level of the singlet first excited electronic state (S_1) to any of vibrational levels of the singlet ground state (S_0). It is because phenolic ring and triazole fluorophores adopt monomer arrangement with the closest centroid long distance (6.658 Å for salt **2** and 5.392 Å for **4**), **Ls** are widely separated by means of entrapment of heavy

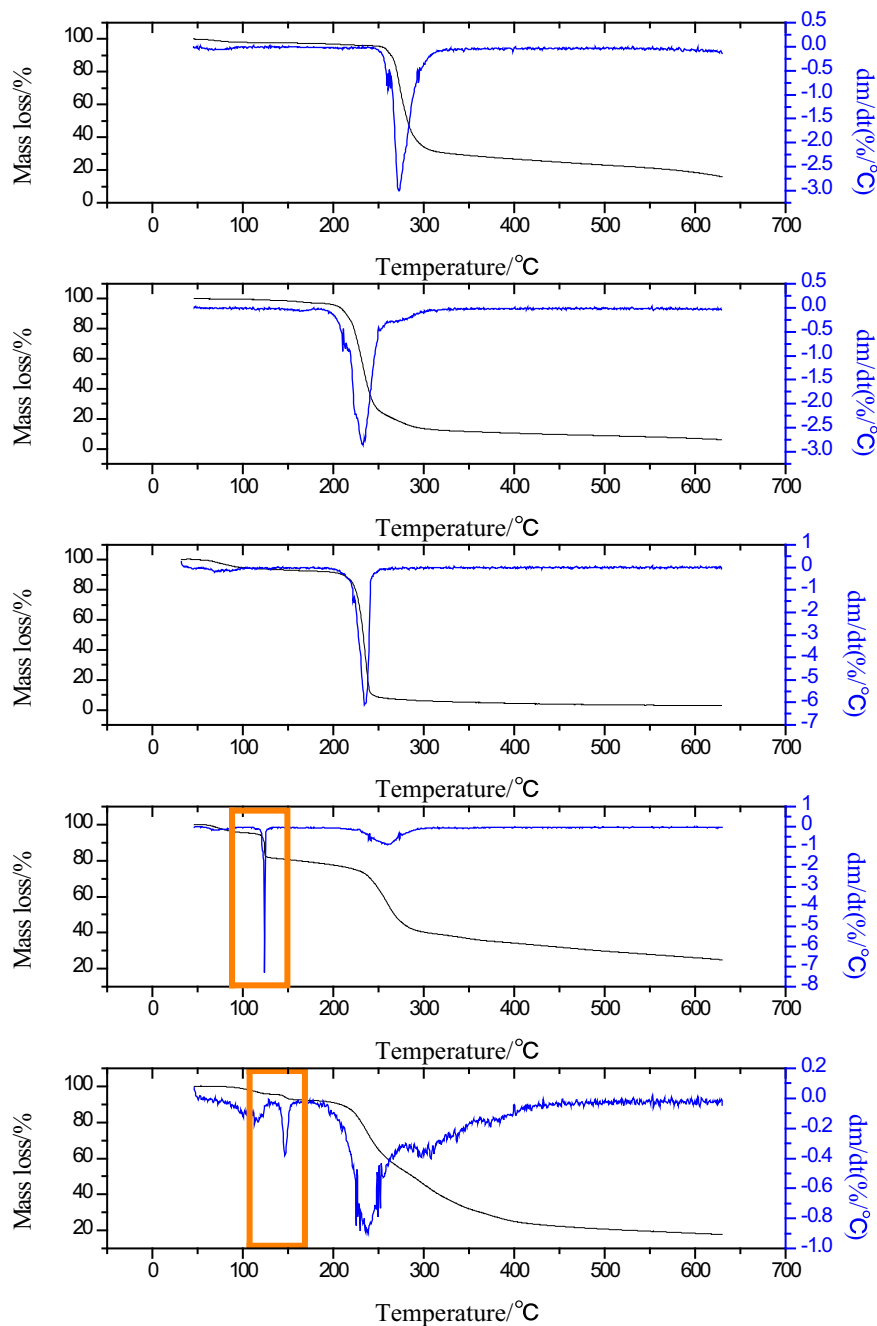


Fig. 7. TGA-DTA profiles of L and four salts.

Table 3
Thermodynamic properties of salts 1–4.

Compound	Decomposition temperature (°C)		Major weight loss transition (°C)	Residual weight loss at 600 (°C) (%) ^c
	T ₁₀ ^a	T ₃₀ ^b		
L		272	250–315	15.9
1		233	200–290	6.1
2		235	210–250	3.2
3	118	240	220–280	10.6
4	125	230	205–370	24.4

^a Temperature at which 10% of weight loss was observed by TGA-DTG.

^b Temperature at which 40% of weight loss occurred in TGA-DTG.

^c Residual weight observed by TGA-DTG at 600 °C in N₂.

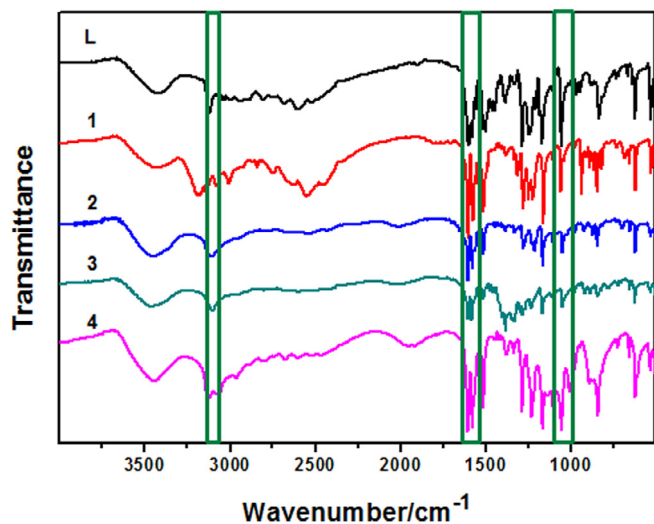


Fig. 8. FT-IR spectra for L and salts 1–4.

anions. The red-shifted and broadening fluorescence spectra of **1** and **3** can be ascribed to the benzene and triazole aggregate because the phenolic and triazole fluorophores form a face-to-face slipped π - π stacked aggregate.

Comparing the fluorescence spectra of the four organic salts in solution and in the solid state indicates that intermolecular interactions and stacking of molecules play an important role in affecting the fluorescence emissions of the four salts. Therefore, to better understand the role of anions in affecting the optical properties in the crystalline state and explore the relationship between the solid state emissions and molecular stacking modes, comparisons of the fluorescence spectra of the salts in the solid state are necessary. These optical properties of salts with different inorganic anions are expected to be useful for the utilization of organic salt-based optoelectronic devices [36].

To evaluate the solid-state fluorescence intensity of the four salts, their emission quantum yields (ϕ_{PL}) were investigated (Table 4). Compared with that of **1** and **3**, the higher ϕ_{PL} values of **2** and **4** could be found, which may be attributed to the suppression of π - π stacking between phenolic and triazole fluorophores by entrapment of heavy anions in the lattices [37].

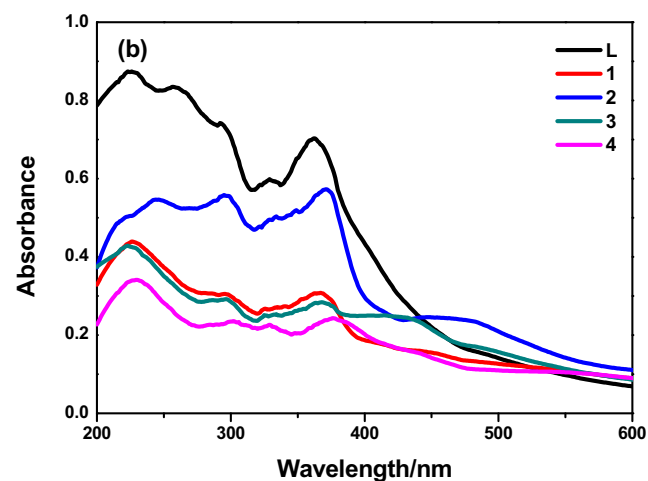
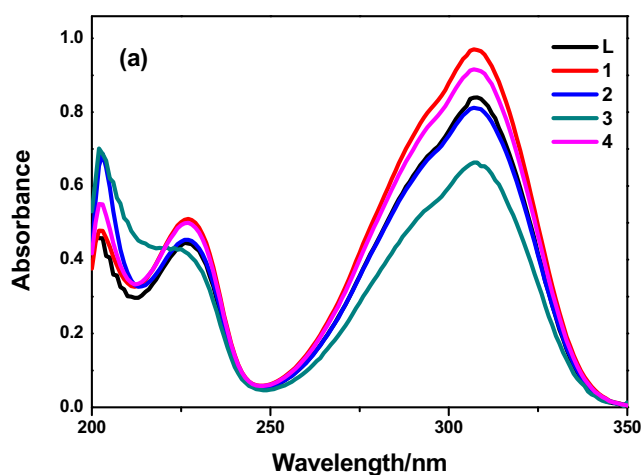


Fig. 9. (a) UV-Vis absorbance (concentration of 10^{-4} g/ml) and (b) diffuse reflectance absorption spectra of L and four salts.

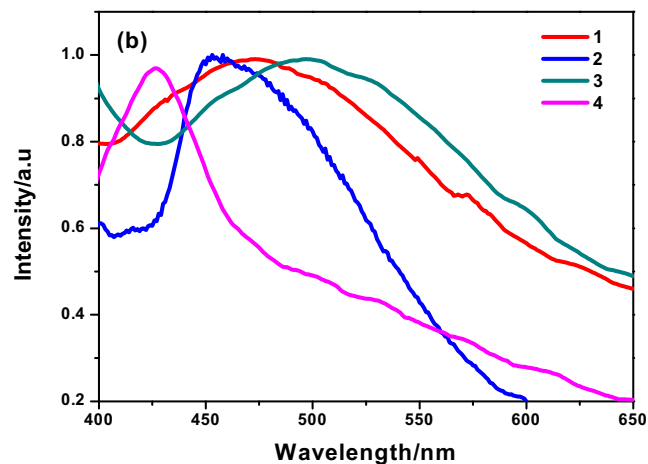
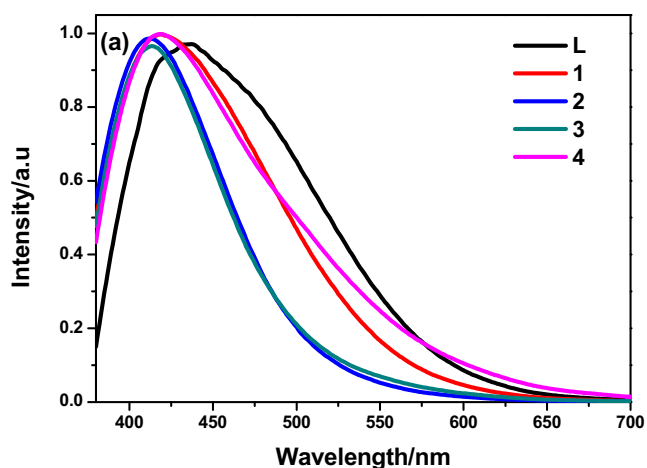


Fig. 10. Fluorescence spectra of (a) L and four salts in solution and (b) 1–4 in solid-state.

Table 4
Photophysical properties of the four salts.

Salt	Solution		Solid	
	Abs (nm)	PL (nm)	PL (nm)	ϕ_{PL} (%)
1	307	423	478	0.08
2	307	412	455	0.15
3	306	413	487	0.06
4	308	421	435	0.14

3. Conclusion

In summary, the molecular interactions and stacking modes of ligand 4-[(4H-1,2,4-triazol-4-ylimino)methyl]phenol have been successfully altered by introducing of different inorganic anions. The obtained organic salts were changing from linear structure to 2D networks. As discussed before, salts in crystalline state were coordinated with N atom of triazole in L [26]. Moreover, the stacking modes of the protonated ligand have shown a close relationship with the solid state fluorescence emissions properties: the face-to-face π -stacked geometries of phenolic ring and triazole resulted in the aggregation-induced red-shifted emissions in salts **1** and **3**, when compared with the monomer arrangement of ligands in **2** and **4**. These results demonstrate that the control of molecular orientation and stacking model play a crucial role in tuning their optical-properties via a salt strategy is an effective way for exploring highly fluorescent derivatives. This strategy can be also employed to tune the emission colors of organic salt chromophores for other luminescent systems, providing a powerful way for designing various new types of organic luminescent materials. Therefore, it may be a useful compound for imaging and other applications [36].

4. Experimental

4.1. Materials

p-Hydroxybenzaldehyde, 4-amino-4(H)-1,2,4-triazoles, hydrobromic acid (HCl), perchloric acid (HClO₄), Nitric acid (HNO₃) and sulfuric acid (H₂SO₄), were all commercially available from Sigma Aldrich and used as received without further purification. Methanol, and ethanol were commercially available from Sinopharm Chemical Reagent Company, Ltd. and used as received without further purification.

4.2. Preparation of 4-[(4H-1,2,4-triazol-4-ylimino)methyl]phenol (L)

The ligand has been reported by others [38] and was prepared according to the following literature procedure: a mixture of 4-amino-1,2,4-triazole (10 mmol), *p*-Hydroxybenzaldehyde (10 mmol) and H₂SO₄ (4 mL) were dissolved in ethanol (50 mL) and were refluxed for 4–10 h. The reaction was monitored through thin layer chromatography. The resulting solvent was evaporated on a rotary evaporator under reduced pressure and residue was washed with ethanol then dried under vacuum. The product compound was recrystallized in ethanol to afford a yellow solid ligand.

4.3. Preparation of organic salts (1–4)

The salts of 4-[(4H-1,2,4-triazol-4-ylimino)methyl]phenol (L) with HCl, HNO₃, HClO₄ and H₂SO₄ were conducted in a slow evaporation crystallization experiment. Organic salts **1–4** were all prepared by mixing the corresponding reactants in 1:1 (2 mmol, HCl, 0.07 g; HClO₄, 0.2 g; HClO₄, 0.13 g; H₂SO₄, 0.20 g; L, 0.38 g) molar ratio into a 20 ml methanol/water (1:1 v/v) solution, and the

resulting solution was kept string for approximately an hour then left to evaporate at room temperature for several days.

4.4. X-ray crystallographic study

The single-crystal X-ray diffraction data of salts **1–4** was collected at a temperature of 293 K using graphite-monochromated Mo K α radiation ($\lambda = 0.071073$ nm) on a Rigaku SCXmini diffractometer (ω -scan technique) [39]. The lattice parameters were integrated using vector analysis and refined from the diffraction matrix. The absorption correction was carried out by the Bruker SADABS program with a multi-scan method. The crystallographic data, data collection and refinement parameters of four salts are summarized in Table 1. The structures were solved by full-matrix least-squares methods on all F^2 data, and used SHELXS-97 and SHELXL-97 programs [40] for structure solution and refinement, respectively. All non-hydrogen atoms were refined anisotropically and hydrogen atoms were geometrically fixed.

4.5. Hirshfeld surface calculations

Molecular Hirshfeld surfaces [41] calculations were conducted by using the CrystalExplorer [42] program, which is a novel method of analyzing intermolecular interactions [27c]. When the cif files of salts **1–4** were input to the CrystalExplorer program, bond lengths of hydrogen were adjusted to typical standard neutron values which can be fully automated. (C–H = 1.083 Å, N–H = 1.009 Å). In this work, the Hirshfeld surfaces were generated using a standard (high) surface resolution. The 3D dnorm surfaces mapped over a fixed color scale of –0.46 (red) to 1.9 Å (blue), 2D fingerprint plots [27] were displayed by using the standard 0.6–2.8 Å view with the *d*_e and *d*_i distance scales displayed on the graph's axes.

4.6. Physical measurements

The four organic salts were characterized by differential scanning calorimetry (DSC) and thermogravimetric analyzes (TGA) were processed using a MettlerToledo TGA/DSC STARE System at a heating rate of 10 K min^{–1} under an atmosphere of dry N₂ flowing at 20 cm³ min^{–1} over a range from 50 to 500 °C, samples were placed in open aluminum oxide crucibles annealed at 1100 °C. The TGA/DSC dates were analyzed by using STARE Software. Infrared spectra of salts **1–4** in the form of potassium bromide pellets were recorded on a SHIMADZU IR prestige-21 FTIR-8400S spectrometer with the spectral range 3800–400 cm^{–1}. UV–Vis absorption spectra were recorded on a Shimadzu UV-3600 spectrometer. Diffuse reflectance spectra were obtained with a Varian Cary 5E spectrometer using barium sulfate (BaSO₄) as a reference. Fluorescence microscopy images were obtained on an Olympus BX51 imaging system. Fluorescence spectra were obtained on a Horiba FluoroMax 4 spectrofluorometer.

Acknowledgements

This work has been supported by the Natural Science Foundation of China (Grant Nos. 21371031 and 21628101), International S&T Cooperation Program of China (No. 2015DFG42240) and the Priority Academic Program Development (PAPD) of Jiangsu Higher Education Institutions.

Appendix A. Supplementary data

CCDC 1524375, 1524377, 1524379 and 1524378 contain the supplementary crystallographic data for salt **1–4**. These data can

be obtained free of charge via <http://dx.doi.org/10.1016/j.poly.2017.05.025>, or from the Cambridge Crystallographic Data Centre, 12 Union Road, Cambridge CB2 1EZ, UK; fax: (+44) 1223-336-033; or e-mail: deposit@ccdc.cam.ac.uk. Supplementary data associated with this article can be found, in the online version, at <http://dx.doi.org/10.1016/j.poly.2017.05.025>.

References

- [1] F. Gao, Q. Liao, Z. Xu, Y. Yue, Q. Wang, H. Zhang, H. Fu, *Angew. Chem. Int. Ed.* 49 (2010) 732.
- [2] D. Yan, J. Lu, J. Ma, M. Wei, D.G. Evans, X. Duan, *Angew. Chem. Int. Ed.* 50 (2011) 720.
- [3] C.A. Strassert, C. Chien, M.D.G. Lopez, D. Kourkoulos, D. Hertel, K. Meerholz, De L. Cola, *Angew. Chem. Int. Ed.* 50 (2011) 946.
- [4] W. Denk, *Proc. Natl. Acad. Sci. U.S.A.* 91 (1994) 6629.
- [5] R.H. Friend, R.W. Gymer, A.B. Holmes, J.H. Burroughes, R.N. Marks, C. Taliani, D. D.C. Bradley, D.A. Dos Santos, J.L. Brédas, M. Lödlund, W.R. Salaneck, *Nature* 397 (1999) 121.
- [6] J.N. Moorthy, P. Venkatakrishnan, P. Natarajan, D.F. Huang, T.J.J. Chow, *Am. Chem. Soc.* 130 (2008) 17320.
- [7] (a) K. Biradha, *CrystEngComm* 5 (2003) 374;
(b) D.V. Soldatov, I.S.J. Terekhova, *Struct. Chem.* 46 (2005) S1;
(c) D. Braga, L. Brammer, N.R. Champness, *CrystEngComm* 7 (2005) 1.
- [8] (a) B.K. An, S.K. Kwon, S. Jung, S.Y.J. Park, *Am. Chem. Soc.* 124 (2002) 14410;
(b) Y.-H. Luo, J.-W. Wang, C. Chen, Y.-J. Li, B.-W. Sun, *Cryst. Growth Des.* 17 (2017) 2576;
(c) Y.-H. Luo, D.-E. Wu, G.-J. Wen, L.-S. Gu, L. Chen, J.-W. Wang, B.-W. Sun, *Chem. Select* 2 (1) (2017) 614.
- [9] (a) J. Chen, C. Law, J. Lam, Y. Dong, S. Lo, D.I. Williams, D. Zhu, B. Tang, *Chem. Mater.* 15 (2003) 1535;
(b) Y.-H. Luo, G.-J. Wen, L.-S. Gu, M.-N. Wang, B.-W. Sun, *Polyhedron* 121 (2017) 101;
(c) Y.-H. Luo, Y. Sun, Q.-L. Liu, L.-J. Yang, G.-J. Wen, M.-X. Wang, B.-W. Sun, *Chem. Select* 1 (13) (2016) 3879.
- [10] N. Schultheiss, A. Newman, *Cryst. Growth Des.* 9 (2009) 2950.
- [11] (a) P. Vishweshwar, J.A. McMahon, J.A. Bis, M.J. Zaworotko, *J. Pharm. Sci.* 95 (2006) 499;
(b) Y.H. Luo, L.J. Yang, Q.L. Liu, Y. Ling, Y. Sun, J.W. Wang, C.Q. You, B.W. Sun, *J. Mater. Chem. C* 4 (2016) 8061.
- [12] (a) C.B. Aakeröy, M.E. Fasulo, J. Desper, *Mol. Pharmaceutics* 4 (2007) 317;
(b) Y.H. Luo, M. Nihei, G.J. Wen, B.W. Sun, H. Oshio, *Inorg. Chem.* 55 (2016) 8147.
- [13] R. Mani, I.B. Rietveld, V. Krishnakumar, M. Louhi-Kultanen, S. Muthu, *J. Phys. Chem. A* 118 (2014) 6883.
- [14] K. Potts, *Chem. Rev.* 61 (1961) 87.
- [15] K.A. Mohamed, R.M. Mohamed, M.A. Mohamed, *Mol. Struct. Theochem.* 959 (2010) 66.
- [16] (a) H. Yuksek, S. Kolayllı, M. Kucuk, M.O. Yuksek, *Indian J. Chem.* 45 (2006) 715;
(b) R. El-Sayed, *Indian J. Chem.* 45 (2006) 738;
(c) B. Kahveci, O. Bekircan, M. Serdar, *Indian J. Chem.* 42 (2003) 1527.
- [17] (a) J. Kothari, M.A. Mehlof, S.P. Singh, S.S. Parmar, V.I. Stenderg, *J. Heterocycl. Chem.* 17 (1980) 1393;
(b) A.K. Sengupta, H.K. Misra, *J. Indian Chem. Soc.* 58 (1981) 508;
(c) H.L. Yale, J.J. Piala, *J. Med. Chem.* 9 (1966) 42.
- [18] (a) D.V. Nadkarni, L.M. Sayre, *Chem. Res. Toxicol.* 8 (1995) 284;
(b) S. Pandeya, D. Sriram, G. Nath, E. DeClercq, *Eur. J. Pharm. Sci.* 9 (1999) 25;
(c) K. Brodowska, E. Lodyga-Chruscinska, *ChemInform.* 46 (2015);
(d) E. Hadjoudis, M. Vittorakis, I. Moustakali-Mavridis, *Tetrahedron* 43 (1987) 1345.
- [19] (a) V.K. Gupta, A.K. Singh, L.K. Kumawat, *Sens. Actuator B-Chem.* 195 (2014) 98;
(b) Y.H. Lau, P.J. Rutledge, M. Watkinson, M.H. Todd, *Chem. Soc. Rev.* 40 (2011) 2848.
- [20] Z.H. Chohan, S.H. Sumrra, M.H. Yousoufi, T.B. Hadda, *Eur. J. Med. Chem.* 45 (2010) 2739.
- [21] (a) I. Anis, Z.N. Aslam, *Int. J. Curr. Pharm. Res.* 5 (2013) 21;
(b) G.Y. Yeap, B.T. Heng, *J. Chem. Sci.* 126 (2014) 247.
- [22] M.X. Liu, T.B. Wei, Q. Lin, Y.M. Zhang, *Spectrochim. Acta A.* 79 (2011) 1837.
- [23] (a) M.J. Sun, H.J. Nie, J.N. Yao, Y.W. Zhong, *Chin. Chem. Lett.* 26 (2015) 649;
(b) E. Giroto, I.H. Bechtold, H. Gallardo, *Liq. Cryst.* 42 (2015) 1798.
- [24] (a) Y. Yu, C.K. Chen, W.C. Law, H. Sun, P.N. Prasad, C. Cheng, *Polym. Chem.* 6 (2015) 953;
(b) K. Ariga, Y. Yamauchi, G. Rydzek, Q. Ji, Y. onamine, K.C.W. Wu, J.P. Hill, *Chem. Lett.* 43 (2014) 36.
- [25] J.G. Haasnoot, *Coord. Chem. Rev.* 131 (2000) 200.
- [26] H.L. Zhou, Y. Cao, *Petrochem. Industry Appl.* 27 (2008) 25.
- [27] (a) Y.-H. Luo, C. Chen, Y.-J. Li, J.-W. Wang, B.-W. Sun, *Dyes Pigments* 143 (2017) 239;
(b) F.P.A. Fabbiani, L.T. Byrne, J. McKinnon, M.A. Spackman, *CrystEngComm* 9 (2007) 648;
(c) J.-W. Wang, Y.-W. Zhang, M.-X. Wang, Y.-H. Luo, B.-W. Sun, *Polyhedron* 124 (2017) 243;
(d) Y.-H. Luo, J.-W. Wang, Y.-J. Li, C. Chen, P.-J. An, S. Wang, C.-Q. You, B.-W. Sun, *CrystEngComm* (2017), <http://dx.doi.org/10.1039/c7ce00693d>.
- [28] G. Socrates, John Wiley & Sons: Chichester, England, 2001.
- [29] (a) K.R. Reddy, A.V. Raghu, H.M. Jeong, Siddaramaiah, *Des. Monomers Polym.* 12 (2009) 109;
(b) Y.P. Zhang, S.H. Lee, K.R. Reddy, A.I. Gopalan, K.P. Lee, *J. Appl. Polym. Sci.* 104 (2007) 2743.
- [30] C. Guillard, S. Horikoshi, N. Watanabe, H. Hidaka, P. Pichat, *J. Photochem. Photobiol. A Chem.* 149 (2002) 155.
- [31] F. Robert, A. D. Naik, B. Tinant, R. Robiette, Y. Garcia, *Chem. – Eur. J.* 15 (2009) 4327.
- [32] K.R. Reddy, H.M. Jeong, Y. Lee, A.V. Raghu *J. Polymer Sci., Part A: Polym. Chem.* 48 (2010) 1477.
- [33] Y.J. Dong, B. Xu, J.B. Zhang, H.G. Lu, S.P. Wen, F.P. Chen, J.T. He, B. Li, L. Ye, W.J. Tian, *CrystEngComm* 14 (2012) 6593.
- [34] (a) S. Kim, Q.D. Zheng, G.S. He, D.J. Bharali, H.E. Pudavar, A. Baev, P.N. Prasad, *Adv. Funct. Mater.* 16 (2006) 2317;
(b) B. Valeur, Wiley-VCH, Weinheim, Germany, 2001;
(c) W. Retting, *Angew. Chem. Int. Ed. Engl.* 25 (1986) 971.
- [35] M. Hassan, E. Haque, K.R. Reddy, A.I. Minett, J. Chen, V.G. Gomes, *Nanoscale* 6 (2014) 11988.
- [36] K.R. Reddy, K.P. Lee, J.Y. Kim, Y. Lee, *J. Nanosci. Nanotech.* 8 (2008) 5632.
- [37] Y. Mizobe, T. Hinoue, A. Yamamoto, I. Hisaki, M. Miyata, Y. Hasegawa, N. Tohnai, *Chem.–Eur. J.* 15 (2009) 8175.
- [38] K.K. Mohammed, S. Salman, S. Muhammad, T. Muhammad, S.S. Muhammad, P. Shahnaz, C.M. Iqbal, *Bioorg. Med. Chem.* 22 (2014) 6509.
- [39] Rigaku, CrystalClear. 2005.
- [40] G.M. Sheldrick, SHELXS97: Programs for Crystal Structure Analysis, University of Göttingen, Germany, 1997.
- [41] (a) S.K. Seth, I. Saha, C. Estarellas, A. Frontera, T. Kar, S. Mukhopadhyay, *Cryst. Growth Des.* 11 (2011) 3250;
(b) S.K. Seth, D. Sarkar, T. Kar, *CrystEngComm* 13 (2011) 4528;
(c) S.K. Seth, *CrystEngComm* 15 (2013) 1772.
- [42] S. K. Wolff, D. J. Grimwood, J. J. McKinnon, D. Jayatilaka, M. A. Spackman, *Crystal Explorer 1.5*, University of Western Australia, Perth, Australia.